GPS Solutions (2025) 29:180
https://doi.org/10.1007/s10291-025-01939-0

RESEARCH

Characterization and performance assessment of the GLONASS ionosphere model

O. Montenbruck[1,2] · C. Price Gonzalez[2] · P. Steigenberger[1]

Received: 19 May 2025 / Accepted: 15 July 2025

Abstract

As part of the ongoing system modernization, the Russian navigation satellite system GLONASS has specified a dedicated electron density model supporting ionospheric path delay corrections for single-frequency navigation users. Solar-geophysical parameters for use with this model are made available through the code division multiple access (CDMA) signals, transmitted by selected GLONASS-K1, -K2 and -M+ satellites on the L3 and L1 frequencies. As a notable feature, the GLONASS ionosphere model can be used to predict the slant total electron content (STEC) through numerical integration of the 3-dimensional electron density along the signal path or a single-layer approximation of the 2-dimensional vertical total electron content (VTEC). Based on reference TEC values provided by global ionosphere maps, the performance of the GLONASS ionosphere model is assessed over an 11-year period using measured solar flux and geomagnetic activity values and compared with correction models of the GPS and Galileo constellations. Furthermore, the quality of solar-geophysical parameters made available in the CDMA navigation message over 1 year after launch of the first GLONASS-K2 satellite is evaluated. Compared to global ionosphere maps of the International GNSS Service, the GLONASS model exhibits VTEC biases in the range of roughly ±1 TECU. Mean absolute errors (MAE) range from about 5 TECU in quiet years to 16 TECU at high solar activity. The corresponding mean absolute percentage errors (MAPE) range from roughly 50% (high activity) to 60% (low activity). Only minor performance differences were observed when comparing predictions based on broadcast values of solar flux and geomagnetic activity with observed values from space weather centers. On the other hand, a clear reduction of both the mean absolute (3–14 TECU) and mean absolute percentage errors (41–45%) is achieved when adjusting the adaptation coefficient of the GLONASS model based on the daily mean ratio of predicted and observed VTEC values. Irrespective of this, major VTEC modeling problems at very high solar activity could be identified. Overall, the GLONASS model outperforms the Klobuchar model but does not reach the prediction performance of the Galileo NeQuick-G and NTCM-G models, which exhibit errors of about 2–8 TECU (MAE) and 26–37% (MAPE).

Keywords GLONASS · Ionosphere · VTEC · STEC

Introduction

Despite a growing share of dual-frequency receivers and the availability of regional correction services from satellite based augmentation systems (SBASs), total electron content (TEC) models remain the primary source for compensating ionospheric path delays in real-time positioning for the majority of mass-market GNSS users. For the different GNSSs, models of different complexity and sophistication are applied along with suitable broadcast parameters.

Within GPS, the United States' Global Positioning System, a computationally-lean single-layer ionosphere model, commonly known as Klobuchar model (Klobuchar 1987; SSC 2022), has been adopted. It describes the global distribution of the vertical total electron content (VTEC) in terms of local time and latitude through a simple parametric model driven by a total of eight polynomial coefficients for modeling the amplitude and extent of the day-side ionospheric bulge. These coefficients are transmitted via the GPS navigation message and routinely updated by the control segment. The Klobuchar model is estimated to

✉ O. Montenbruck
oliver.montenbruck@dlr.de

[1] Deutsches Zentrum für Luft- und Raumfahrt, German Space Operations Center, 82234 Weßling, Germany

[2] Technische Universität München, 80333 Munich, Germany

Published online: 28 July 2025

provide a roughly 50% root-mean-square (RMS) reduction of the ionospheric range error worldwide (Klobuchar and Kunches 2003; Orús et al. 2002), making it effective for many applications but insufficient, if higher accuracy is needed. For commonality with GPS, it has also been adopted by other global and regional navigation satellite systems including the Chinese BeiDou-2/3 system, the Japanese Quasi-Zenith Satellite System (QZSS), and the Navigation with Indian Constellation (NavIC) system. As part of their legacy navigation messages, these constellations offer dedicated coefficients for the Klobuchar model aiming at improved corrections in the respective service areas.

For the European Galileo system, a notably more complex ionosphere model (NeQuick-G; EU 2016) has been selected, which offers a fully 3-dimensional (3D) description of the electron density. The model is driven by the "effective ionization level" Az, which replaces the solar radio flux $F_{10.7}$ as a measure of solar activity and is routinely determined by the Galileo control segment from observations to best fit the actual state of the ionosphere. Coefficients of a second-order polynomial describing a latitude-dependent Az are provided through the Galileo navigation messages with roughly half-daily updates. The slant total electron content (STEC) in NeQuick-G is computed through numerical integration of the local electron density along the line of sight, which allows use of the model for generic user locations, including even spaceborne receivers (Montenbruck and González Rodríguez 2020). However, the improved flexibility and modeling accuracy of NeQuick-G come at the expense of a notably higher computational effort than for the Klobuchar model. To cope with this limitation, NTCM-G (Neustrelitz Total electron Content Model – Galileo; EU 2022; Hoque et al. 2019) is offered as an alternative to NeQuick-G for Galileo users. NTCM-G makes use of the same activity parameters as NeQuick-G but provides a 2-dimensional (2D) representation of the global vertical total electron content (VTEC) based on which the slant TEC can be obtained via a modified single-layer mapping function. Compared to the GPS Klobuchar model, NTCM-G offers a notably more realistic representation of the regional VTEC distribution, which even includes the modeling of the equatorial crests.

To cope with the limited accuracy of the Klobuchar model, a new BeiDou Global Ionospheric delay correction Model (BDGIM; CSNO 2017; Wang et al. 2021) has been introduced for the third-generation BeiDou global navigation system. BDGIM uses a set of nine broadcast parameters to describe the global VTEC distribution through a low-order spherical harmonic approximation, based on which the STEC can again be computed with a single-layer mapping function. Similar to the Klobuchar model and NTCM-G, BDGIM is computationally lean but limited to users near the surface of the Earth.

Following GPS, the Russian Globalnaja Nawigazionnaja Sputnikowaja Sistema (GLONASS) was the second satellite navigation system offering a global navigation service. With civil signals in the L1 and L2 frequency bands, there was formally no need for considering a ionospheric correction model as part the signal specification, even though the majority of GLONASS-capable receivers was long limited to single-frequency processing. In fact, a ionospheric correction model for GLONASS users was only introduced in 2016 as part of the ongoing GLONASS modernization effort and the introduction of code division multiple access (CDMA) signals on the L1, L2, and L3 frequencies (Russian Space Systems 2016c). The new GLONASS ionosphere model is driven by three parameters that are included in string type 25 of the L1OC and L3OC CDMA navigation messages. These comprise a pair of solar and geomagnetic activity data ($F_{10.7}$, A_p) as well as an "adaptation coefficient" c_A, which serves as a global scale factor for the modeled electron density. While specified already in 2016, a preliminary navigation message format was used in L3 CDMA transmission of GLONASS-M+ and early K1 satellites for many years. Actual transmissions of ionosphere model parameters have presumably been initiated in the 2021–2023 time frame even though the exact start time is not known due to a lack of monitoring sites supporting reception and extraction of the new CDMA messages. While initially confined to a small set of GLONASS-K1 and -K2 satellites, the transmission of solar-geomagnetic activity parameters for the GLONASS ionosphere model was extended to five GLONASS-M+ satellites in late 2024.

Similar to NeQuick-G, the GLONASS ionosphere model provides a fully 3-dimensional description of the electron density and can thus be used for STEC computation at arbitrary user locations. On the other hand, the specific height profile adopted in the model also offers a closed-form solution for the VTEC distribution. Along with a standard mapping function, STECs for terrestrial users can thus be computed in a single-layer approximation, rather than a numerical integration along the signal path. The hybrid 2D/3D nature distinguishes it from other models and makes the GLONASS model of interest for a wider range of GNSS positioning applications. Initial analyses described in Ivanov et al. (2017) and Yasyukevich et al. (2023) indicate a competitive range correction performance of the GLONASS model, but have been conducted prior to the availability of broadcast ionosphere parameters and relied exclusively on external solar-geomagnetic activity data.

With the above background and motivation, we provide an independent assessment and characterization of the GLONASS ionosphere model and compare its performance with that of the GPS and Galileo models. Following an overview of the GLONASS model concept and architecture, a 1-year performance analysis using broadcast ionosphere parameters as transmitted by selected GLONASS-K1, -K2, and -M+

satellites is provided. For an improved characterization over a wider range of ionospheric conditions, complementary results covering roughly one solar cycle are presented based on recorded solar-geomagnetic activity data from space weather service centers. Finally, the potential of improving the model accuracy through adjustment of the hitherto unused adaptation coefficient is evaluated.

GLONASS ionosphere model architecture

The GLONASS model describes the ionospheric electron density n_e at a given time and location as a function of

- the calendar month ($m = 1, \ldots, 12$) and the Universal Time (UT),
- the geographic longitude λ, latitude φ, and altitude h, as well as
- the solar radio flux $F_{10.7}$ at 10.7 cm, the daily geomagnetic activity index A_p, and the adaptation coefficient c_A.

Auxiliary quantities derived from these input parameters comprise

- the local time LT,
- the declination $\delta_\odot$ of the Sun,
- the geomagnetic longitude λ_m and latitude φ_m, as well as the associated dip angle $i = \tan^{-1}(2\tan(\varphi_m))$.

For the latter quantities, a centered dipole model (Laundal and Richmond 2017) with coordinates $\lambda_{NP} \approx -68.75°$ and $\varphi_{NP} = \approx +78.46°$ of the magnetic North pole is employed. Within the GLONASS Interface Control Document (ICD; Russian Space Systems 2016c), rounded values of $\cos(\varphi_{NP})$ and $\sin(\varphi_{NP})$ are provided for the computation of the geomagnetic coordinates, which may cause range violations for the arguments of inverse trigonometric functions. Users are therefore advised to consider rigorous expressions of the respective values to enable flawless application of the GLONASS ionosphere model at arbitrary locations.

Given the dominating contribution of the F2 layer, the GLONASS ionosphere model focuses on the representation of the spatial and temporal variation of the F2 peak electron density, which is described by a product

$$N_{\max,F2} = 0.66 \cdot 10^{11} \mathrm{e}^-/\mathrm{m}^3 \cdot D \cdot E \cdot F \cdot G \cdot H \cdot I \cdot J \,. \quad (1)$$

The individual contributions

$$\begin{aligned} &D(\mathrm{LT}, \delta_\odot, \varphi_m) \\ &E(\mathrm{LT}, m, \varphi_m, F_{10.7}) \\ &F(\mathrm{LT}, m, \varphi_m, F_{10.7}) \\ &G(\varphi_m, F_{10.7}) \\ &H(\lambda_m, \varphi_m) \\ &I(m, \varphi_m, i, F_{10.7}) \\ &J(\mathrm{LT}, \delta_\odot, m, \varphi_m, F_{10.7}) \end{aligned} \quad (2)$$

are formulated as analytical functions of the respective parameters and capture daily, seasonal, and regional variations of the peak electron density as well as its dependency on solar activity.

Complementary F2 layer parameters include the altitude

$$h_{\max,F2}(LT, m, \delta_\odot, \varphi_m, F_{10.7}) \quad (3)$$

(in [km]) of the peak electron concentration, the critical frequency

$$f_{0,F2} = \sqrt{\frac{N_{\max,F2}}{0.124 \cdot 10^{11} \mathrm{e}^-/\mathrm{m}^3}}\,\mathrm{MHz} \quad (4)$$

associated with the F2 peak, and the dimensionless transmission factor

$$M(3000)_{F2} = \frac{1490\,\mathrm{km}}{h_{\max,F2} + 176\,\mathrm{km}}\,, \quad (5)$$

which gives the ratio $f_{3000,F2}/f_{0,F2}$ of the highest frequency $f_{3000,F2}$ that can be received at a distance of 3,000 km upon refraction in the ionosphere and the F2 critical frequency (Bilitza et al. 2022). They are jointly used to obtain the scale heights

$$B_{bot}(N_{\max,F2}, f_{0,F2}, M(3000)_{F2}) \quad (6)$$

and

$$B_{top}(m, B_{bot}, h_{\max,F2}, N_{\max,F2}, F_{10.7}) \quad (7)$$

of the electron density profile below and above the F2 peak altitude based on expressions inherited from the family of NeQuick models (Leitinger et al. 2005). Similar to NeQuick-1 and -G, the GLONASS model involves different expressions for the topside scale height covering the periods from April to September and October to March, respectively, rather than using the unified formulation of NeQuick-2 (Nava et al. 2008). It may be noted, though, that the GLONASS model adopts a different constant (i.e., 0.1 instead of 0.14 in NeQuick-1/G) for the solar-flux dependence of B_{top} in the summer season.

Subject to high geomagnetic activity as characterized by values $A_p > 27$, the F2 peak electron density is scaled by a correction factor

$$c_N(\mathrm{LT}, m, \varphi, \varphi_\mathrm{m}, F_{10.7}, A_p) \tag{8}$$

which accounts for atmospheric temperature variations under the influence of geomagnetic disturbances and is formulated as an analytical function of local time, season, geographical location, and solar activity. Along with this, the F2 peak height is incremented by a correction

$$c_h(\varphi_\mathrm{m}, A_p) \tag{9}$$

and the bottom and top layer scale heights computed so far are multiplied with correction factors

$$\begin{aligned} c_{B\mathrm{top}} &= (1 - \log(c_N)) \\ c_{B\mathrm{bot}} &= (1 - 0.5 \cdot \log(c_N)) \end{aligned} \tag{10}$$

to account for geomagnetic variations of the ionosphere at $A_p > 27$.

Finally, the model allows for scaling of the peak electron density with the adaptation factor c_A. Since the electron density n_e at any user location is itself proportional to $N_{\mathrm{max,F2}}$, the adaptation factor acts as a global scaling factor for the modeled TEC values. This opens the possibility for adjusting modeled electron densities or total electron contents to observed values without modifying the $F_{10.7}$ and A_p values. Possible systematic modeling errors that might arise in selected periods or under specific space weather conditions can thus be compensated by the control segment, if needed.

The vertical electron density profile in the GLONASS ionosphere model is described by two semi-Epstein layers functions (Bilitza et al. 2022) covering the altitude range up to and above the F2 peak height, respectively. For the bottom layer, the lower half of an Epstein profile

$$n_e = 4N_{\mathrm{max,F2}} \cdot \frac{e^x}{(1+e^x)^2} \quad \text{with} \quad x = \frac{h - h_{\mathrm{max,F2}}}{B_{\mathrm{bot}}} \tag{11}$$

with a fixed scale height is used, while the topside density model

$$n_e = 4N_{\mathrm{max,F2}} \cdot \frac{e^z}{(1+e^z)^2} \tag{12}$$

with

$$z = \frac{y}{1.0 + \dfrac{12.5 \cdot y}{100.0 + 0.1 \cdot y}} \quad \text{and} \quad y = \frac{h - h_{\mathrm{max,F2}}}{B_{\mathrm{top}}} \tag{13}$$

includes an additional scale height gradient. Except for a slightly inconsistent constant (0.1 instead of 0.125) the topside profile function matches the formulation of Leitinger et al. (2005), which has been adopted in both the NeQuick-1 and -G models (Bidaine and Warnant 2010). The resulting

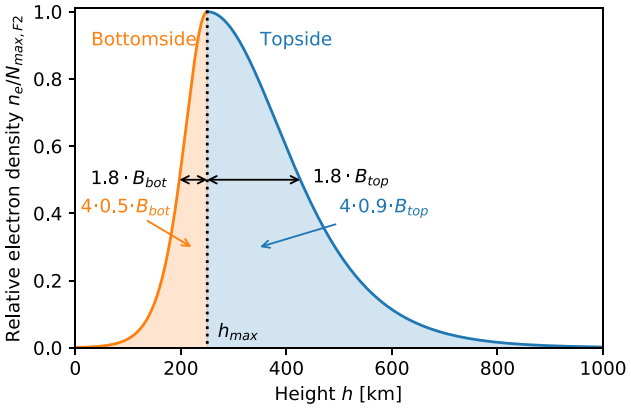

Fig. 1 Schematic view of the electron density profile adopted in the GLONASS ionosphere model for a peak height of 250 km as well as bottom/top layer scale heights of 20 and 100 km, respectively. Annotations illustrate the dependence of the profile width and integrals on the scale heights of the two layers

electron density profile is illustrated in Fig. 1. Its peak density is attained at $h_{max,F2}$ and the distribution exhibits a full-width-half-maximum (FWHM) of about $1.8 \cdot (B_{\mathrm{bot}} + B_{\mathrm{top}})$.

Based on the analytical expressions for the 3D electron density distribution, the slant TEC between an arbitrary user location and the transmitting satellite can be obtained through numerical integration along the line of sight. In the absence of dedicated recommendations or specifications in the GLONASS CDMA ICD (Russian Space Systems 2016c), the choice of a numerical integration method for this purpose is ultimately left to the user's discretion. Following the example of NeQuick-G, which likewise obtains the slant TEC through integration of the 3D electron distribution, we adopt a 15-point Gauss-Kronrod integration as described in EU (2016) for the present study. In accord with that reference, the entire signal path is divided into distinct segments below 1000 km, between 1000 and 2000 km, and above 2000 km to obtain a reasonable distribution of grid points for the GLONASS electron density integration.

As an alternative to the generic, but computationally demanding STEC integration between arbitrary points, a semi-analytical approximation for the VTEC of a ground-based user location is provided as part of the GLONASS ionosphere model. Making use of the analytical integral

$$\int_{-\infty}^{0} \frac{e^x}{(1+e^x)^2} dx = 0.5 \tag{14}$$

of the Epstein function and the numerical solution

$$\int_{0}^{\infty} \frac{e^{z(y)}}{(1+e^{z(y)})^2} dy \approx 0.908\,, \tag{15}$$

for the modified topside profile, the total electron content above ground is approximated by the expression

$$\begin{aligned} \mathrm{VTEC} &= \int_0^\infty n_e(h)dh \\ &\approx 4N_{\mathrm{max,F2}} \cdot (0.5 \cdot B_{\mathrm{top}} + 0.9 \cdot B_{\mathrm{top}}) \, . \end{aligned} \tag{16}$$

In combination with a suitable mapping function $M(z)$, where z denotes the zenith angle of the observed GLONASS satellite at the user location, the slant TEC can then be expressed as

$$\mathrm{STEC} = \mathrm{VTEC} \cdot M(z) \, . \tag{17}$$

For the 2D formulation of the GLONASS ionosphere model, the common single-layer mapping function

$$M(z) = \frac{1}{\sqrt{1 - \left(\frac{\sin(z)}{1 + h_{\mathrm{ion}}/R_\oplus} \right)^2}} \tag{18}$$

with Earth radius $R_\oplus$ and a shell height of $h_{\mathrm{ion}} = 400\,\mathrm{km}$ is adopted. Evidently, the 2D formulation offers a notably reduced computational effort, since the parameters of the vertical electron density profile need to be computed only once for a given location, but is limited to users at or near the Earth's surface. Aside from this limitation, the GLONASS ICD highlights the occurrence of increased TEC errors at elevations below 30° when using the 2D formulation of the GLONASS ionosphere model. In this context, it is also worth mentioning, that the VTEC in the 2D model is expected to be computed at the user location rather than the ionospheric pierce point, which is commonly used in other single-layer models. As such, a single VTEC computation is sufficient for modeling ionospheric path delays of all tracked satellites irrespective of their zenith angle, but regional VTEC gradients are evidently ignored.

A sample VTEC map obtained with the GLONASS ionosphere model is shown in Fig. 2 along with a global ionosphere map (GIM) or the International GNSS Service (IGS; Johnston et al. 2017) and predictions of other models. Compared to the Klobuchar and NTCM model, the GLONASS model achieves a higher regional resolution of TEC variations, which reflects the larger number and increased complexity of the individual model functions used to describe the global electron density variation (cf. Eqs. 1 and 2). On the other hand, the model is apparently outperformed by NeQuick-G which offers yet a higher granularity in the description of small-scale VTEC variations.

The varying complexity of the individual models is also reflected in a notably different computational effort. This is illustrated by relative execution times of repeated STEC computations based on C++ software implementations of the various models prepared by the authors. A fairly similar run-time performance is obtained for the three single-layer models, while a two to three orders of magnitude higher effort is required for the 3D formulations using numerical integration of the electron density along the signal path (Table 1). In terms of absolute computing times, values between about 1 μs for the single-layer models and about 1 ms for the most demanding model were required on a desktop computer with an i7-8665U processor operated at a 1.9 GHz clock rate.

Compared to NeQuick-G, the GLONASS ionosphere model still requires a 4–5 times lower processing effort using the same integration technique and tolerances. It thus lends itself as a potential alternative for, e.g., space applications with tight computational resources. A related advantage concerns the fact that the GLONASS model makes exclusive use of analytical expressions and does not require external data tables as used in the NeQuick-G model for interpolation of the modified dip latitude as well as the F2 critical frequency $f_{0,\mathrm{F2}}$ and obliquity factor $M(3000)_{\mathrm{F2}}$.

Space weather data

Ionospheric activity parameters transmitted by the GLONASS constellations were recorded for this study over a 1-year time frame (January to December 2024) by a set of two JAVAD TRE_3S receivers using a prototype firmware capable of logging the new GLONASS L1OC and L3OC CDMA navigation messages (Steigenberger et al. 2024). Ionospheric activity parameters from string type 25 providing Earth orientation and ionosphere model parameters (Russian Space Systems 2016a, b) were extracted from the raw navigation data bits and stored in the latest version 4.02 of the Receiver Independent Exchange format (RINEX; Gini 2024).

Overall, the ionospheric parameters were transmitted by the three latest K1B satellites (space vehicle numbers (SVN) R805, R806, R807) and the first K2 satellite (R803) between January and mid November 2024. Thereafter, the transmission was extended to five out of six GLONASS-M+ satellites (R855, R856, R858, R859, and R860). With two stations located in central Europe (Oberpfaffenhofen, Germany) and Australia (Sydney, New South Wales), it is not possible to achieve a fully continuous coverage of these satellites, but any changes of activity parameters encountered during the visibility periods were recorded and logged in the RINEX navigation data files.

For comparison with the broadcast values, actual space weather data collected and distributed by the Helmholtz Centre for Geosciences (GFZ) were used (GFZ 2025; Matzka et al. 2021b). These comprise the observed local noon-time solar radio flux $F_{10.7}$ in solar flux units ($1\,\mathrm{sfu} = 1 \cdot 10^{-22}\,\mathrm{Wm^{-2}Hz^{-1}}$) as provided by the Dominion Radio Astrophysical Observatory and Natural Resources Canada (Tapping 2013) as well as the dimensionless daily

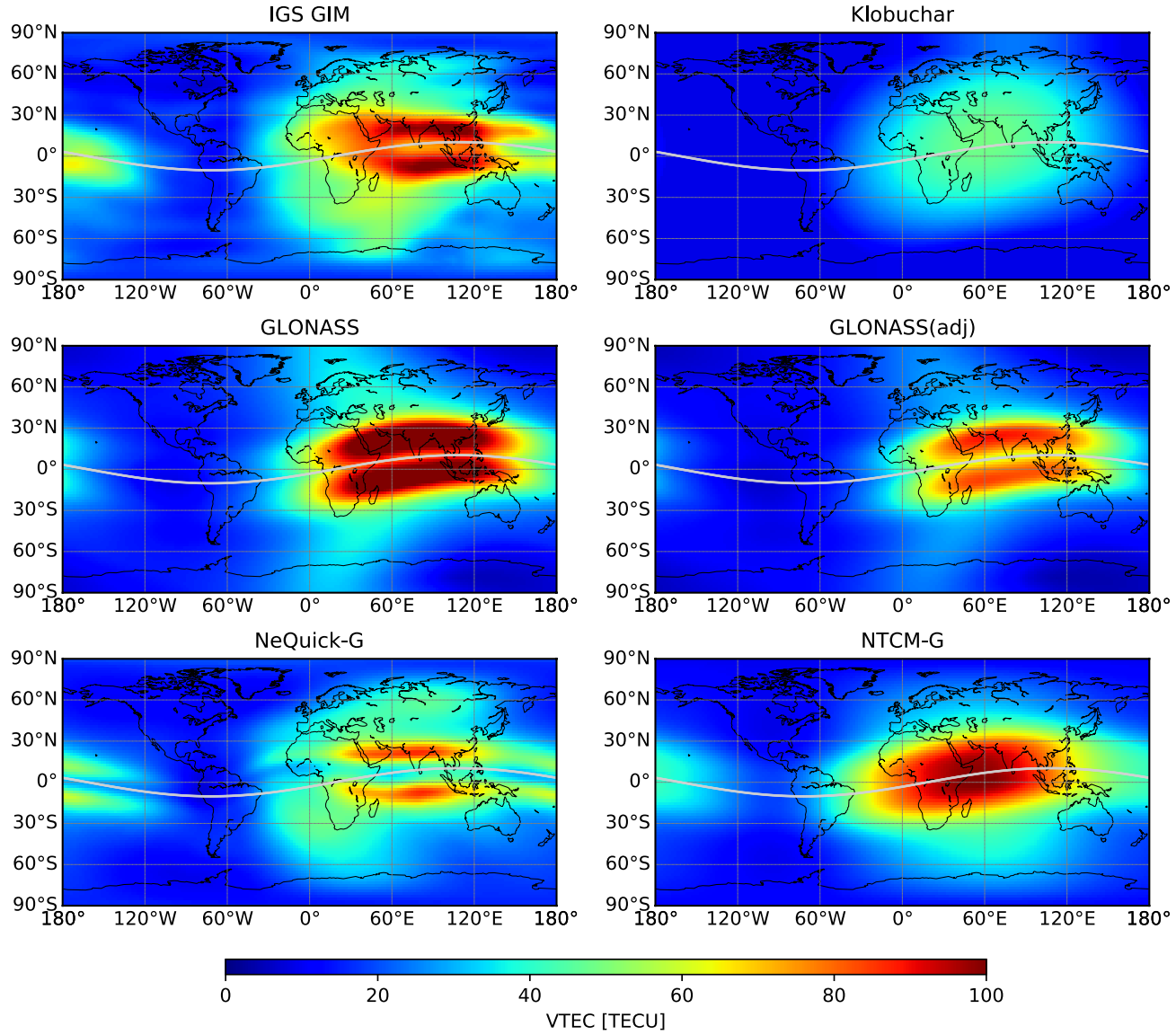

Fig. 2 VTEC maps for 15 March 2024, 10:00 UT, obtained with the Klobuchar, GLONASS, NeQuick-G and NTCM-G models. For comparison, the observed VTEC as given in the global ionosphere map (GIM) of the International GNSS Service (IGS) for the same epoch is shown (top left). For the GLONASS model, results for both the nominal adaptation coefficient ($c_A = 1.0$; center left) and an adjusted value of $c_A = 0.75$ for the winter period (center right) are given

Table 1 Computing times for STEC computation with different ionosphere models relative to NTCM-G

Model	Processing time
Klobuchar	0.6
NTCM-G	1 (ref)
GLONASS (2D)	1.0
GLONASS (3D)	160
NeQuick-G	770

equivalent planetary amplitude A_p produced by GFZ's Niemegk geomagnetic observatory (Matzka et al. 2021a).

Solar-geomagnetic activity parameters as transmitted by the GLONASS satellites for ionospheric path delay correction are compared in Fig. 3 with observed $F_{10.7}$ and A_p values from the space weather services over a 2-month period in 2024. The broadcast solar flux values follow the overall trend of the observed values, but indicate a 1–2 day lag with respect to data of the space weather services, which likely relates to filtering and prediction of measured solar-geomagnetic activity parameters in the GLONASS ground segment.

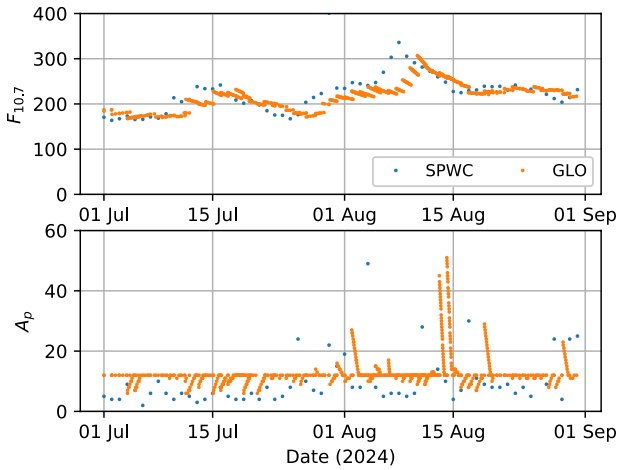

Fig. 3 Comparison of GLONASS broadcast ionosphere parameters (GLO) with observed solar-geomagnetic activity parameters from global space weather centers (SPWC) for a 2-month period in 2024

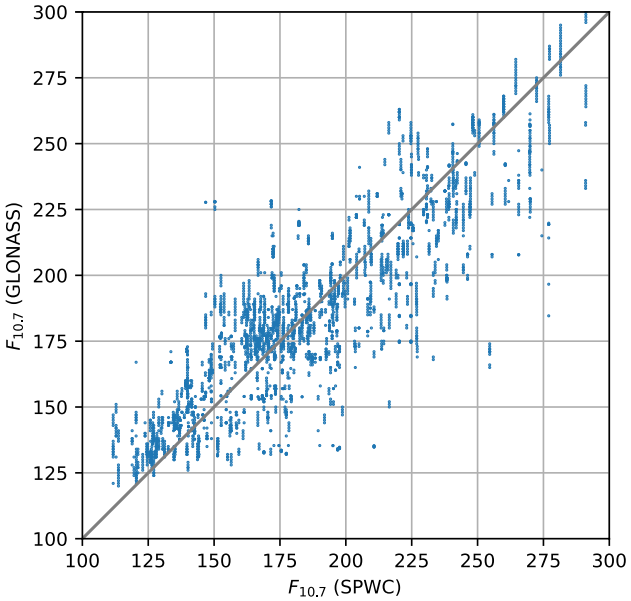

Fig. 4 Scatter plot comparing the GLONASS broadcast solar flux values with space weather center (SPWC) reference data in 2024

Overall, the broadcast solar flux values exhibit a mean percentage difference of less than 1% and a mean absolute percentage difference of 9% compared to the space weather center reference values in the 2024 data interval (Fig. 4).

Individual CDMA navigation messages provide a single set of ionospheric parameters applicable from the time of first transmission. These are repeatedly updated throughout a day and linear trends over intervals of 1–2 days can be observed in the ionospheric parameters transmitted by individual satellites, before a step-wise change is encountered. These empirical observations suggest that the $F_{10.7}$ values are derived onboard the satellite from linear predictions that are precomputed on ground and refreshed, whenever a new batch of ephemeris data is uploaded to a satellite by the control segment. Individual satellites receive their uploads at different times, which finally gives rise to inconsistent ionospheric activity parameters transmitted concurrently. These show up in Fig. 3 as multiple trend lines with overlapping time intervals. Similar to other GNSSs that do not provide a dedicated age-of-data information for ionosphere model coefficients, the actual choice of the parameter set used for evaluating ionospheric path delay corrections is ultimately left to the discretion of the user. Within the present study, the GLONASS broadcast ionosphere parameters with the latest time of first transmission prior to the analysis epoch are used in accordance with the general conventions of the BRD4 RINEX4 navigation data product (Montenbruck and Steigenberger 2022).

The geomagnetic activity parameters transmitted in the L1OC and L3OC navigation messages are mostly confined to values below the threshold ($A_p = 27$) for the application of geomagnetic activity corrections in the GLONASS model. A standard value of $A_p = 12$ is transmitted for a dominating fraction of all epochs and phases of reduced or increased geomagnetic activity show a largely linear trend towards this value. In the course of 2024, the broadcast A_p indices exhibit a mean percentage difference of 85% relative to reference data from the Niemegk observatory, which means that the transmitted values are roughly a factor of two larger than expected. As mentioned in Matzka et al. (2021a), the A_p index can be multiplied by 2 nT to approximate the average geomagnetic disturbance at 50° geomagnetic latitude. This raises concerns, whether the broadcast values transmitted in the navigation messages are indeed A_p indices (as stated in the message definition in Russian Space Systems (2016a, b)) or possibly equivalent magnetic field strengths in units of [nT] as mentioned in selected places of the GLONASS ionosphere model description. However, no clarification can presently be received from the GLONASS system provider. The ICD message definition has therefore been applied without modification, and the broadcast A_p values are consistently interpreted as indices throughout this study. In particular published A_p indices are used when driving the GLONASS ionosphere model with external space weather data in periods prior to the transmission of broadcast ionosphere parameters.

Finally, we note that the values of the adaptation coefficient c_A were set to one in all CDMA navigation records received in the 2024 time frame. Apparently, no effort is presently made by the control segment to tune this parameter for an optimized match of observed and predicted total electron content values at the given solar-geomagnetic activity.

Data and analysis concept

Common approaches for the validation of ionospheric models or products comprise the comparison of VTECs with GIMs or VTEC measurements of altimeter satellites, the comparison of STECs with measured path delays from dual-frequency observations of selected ground stations, as well as the analysis of single-frequency positioning results (Hernández-Pajares et al. 2009; Roma-Dollase et al. 2018; Wielgosz et al. 2021; Li et al. 2023; Xu et al. 2025; Milanowska et al. 2025). For the performance characterization of the GLONASS ionosphere model, we focus on the assessment of VTEC errors relative to GIMs of the IGS. Compared to measured STEC, the use of GIMs avoids the need for independent calibration of differential code biases and is most efficient for comparisons covering extended time periods and a global set of sample points. The same approach has been applied in previous studies (Ivanov et al. 2017; Yasyukevich et al. 2023) and is well suited for identifying the gross performance differences between individual models.

The IGS0OPSFIN product used as the reference for our study represents a weighted average of GIMs from individual analysis centers. Their accuracy has been evaluated using altimeter-derived VTEC measurements from Jason satellites as well as direct comparison with site-specific STEC measurements. Differences between the IGS GIMs and Jason VTEC values exhibit biases at the level of up to ±2 TECU, i.e. $2 \cdot 10^{16}\,\mathrm{e}^-/\mathrm{m}^2$, and standard deviations of 2–7 TECU depending on latitude and solar activity, while STECs predicted from GIMs differ from measured STEC values by typically less than 3 TECU RMS (Wielgosz et al. 2021; Roma-Dollase et al. 2018; Li et al. 2023).

Four different statistical metrics are employed for a quantitative description of absolute and relative model errors:

– The mean error measures the systematic deviation of a model's TEC predictions from the reference and is computed as

$$\mathrm{ME} = \frac{1}{N}\sum_{i=1}^{N}\left(\mathrm{TEC}_{\mathrm{model},i} - \mathrm{TEC}_{\mathrm{ref},i}\right), \tag{19}$$

where N is the total number of data points, $\mathrm{TEC}_{\mathrm{model},i}$ represents the TEC value computed by the model, and $\mathrm{TEC}_{\mathrm{ref},i}$ is the reference TEC value. The mean error is also designated as TEC bias. When using IGS GIMs or measured TEC values from dual-frequency observations as a reference, different biases may arise depending on the specific choice of differential code biases in the determination for the reference values.

– The Mean Absolute Error

$$\mathrm{MAE} = \frac{1}{N}\sum_{i=1}^{N}\left|\mathrm{TEC}_{\mathrm{model},i} - \mathrm{TEC}_{\mathrm{ref},i}\right| \tag{20}$$

quantifies the average magnitude of error, regardless of its sign. Similar to the RMS error, it provides a measure of the typical deviation between model outputs and reference values irrespective of the TEC value itself but is less sensitive to outliers. The MAE translates into ionospheric delay errors of 0.16 m/TECU at the L1 frequency, thus indicating the magnitude of the pseudorange modeling and positioning errors in single-frequency navigation.

– The Mean Percentage Error

$$\mathrm{MPE} = \frac{100\%}{N}\sum_{i=1}^{N}\frac{\mathrm{TEC}_{\mathrm{model},i} - \mathrm{TEC}_{\mathrm{ref},i}}{\mathrm{TEC}_{\mathrm{ref},i}} \tag{21}$$

evaluates the average relative bias and is indicative of a systematic scaling error of the modeled TEC values. MPE statistics may be affected by samples with small reference TEC values and needs to be handled with due care during low solar activity. Within the subsequent analysis, a lower threshold of 1 TECU is considered in the MPE computation to avoid an undue impact of near-zero reference TEC values.

– The Mean Absolute Percentage Error, finally, measures the average magnitude of the relative bias:

$$\mathrm{MAPE} = \frac{100\%}{N}\sum_{i=1}^{N}\left|\frac{\mathrm{TEC}_{\mathrm{model},i} - \mathrm{TEC}_{\mathrm{ref},i}}{\mathrm{TEC}_{\mathrm{ref},i}}\right| \tag{22}$$

Its complement, PER = 100% − MAPE, is often used as an alternative performance indicator for the overall accuracy or correction capability of a given ionosphere model. Similar to the MPE, a lower threshold of 1 TECU is considered for the reference TEC in the MAPE analysis for this study.

Model-based and GIM VTEC values were evaluated on a daily basis with 1 h sampling for a total of 30 sites coinciding with actual monitoring stations of selected GNSS networks (Fig. 5). Roughly one third each of these sites are located in the three bands of low ($|\varphi_\mathrm{m}| \le 30°$), medium ($30° < |\varphi_\mathrm{m}| \le 60°$) and high ($60° < |\varphi_\mathrm{m}|$) geomagnetic latitude. Statistics of model errors were then obtained for a total of 11 years from 2014 to 2024, covering essentially the time between the maxima of solar cycles 24 and 25.

For the characterization of the GLONASS model itself, three different use cases are considered:

– First, the operational model performance is evaluated using the activity parameters ($F_{10.7}$, A_p, and c_A) actually transmitted in the CDMA navigation messages.

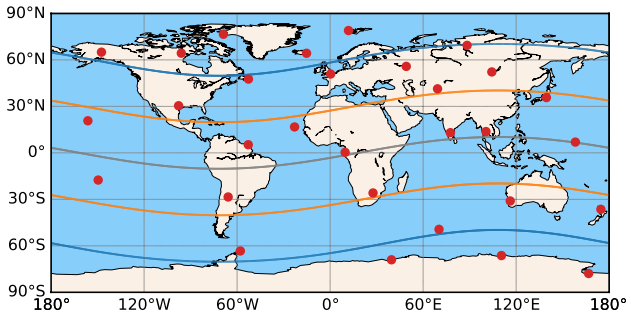

Fig. 5 World map showing the location of test sites (AUT0, BAKE, CAS1, CATA, CHOF, CPVG, CUSV, FAA1, FAIR, HERT, HOFN, HRAG, IISC, IRKJ, KERG, KOUR, KZN2, MAO0, NKLG, NNOR, NRIL, NYA1, OHI3, POHN, SCTB, STJO, SYOG, TASH, THU2, WARK) for evaluation of VTEC errors. Solid lines indicate the geomagnetic equator (grey) as well as geomagnetic latitudes of ±30° (orange) and ±60° (blue)

Given the limited availability of such data, the respective statistics are restricted to the final year (2024) of our overall analysis period.

- Secondly, solar-geomagnetic activity data from space weather service providers (GFZ 2025) are used as a substitute for the broadcast values to drive the model. The extended availability offers a full coverage of an entire solar cycle.
- Finally, synthetic adaptation coefficients

$$c_A = \left(\frac{1}{N} \sum_{i=1}^{N} \frac{\mathrm{TEC}_{\mathrm{model},i}}{\mathrm{TEC}_{\mathrm{ref},i}} \right)^{-1} = \frac{1}{1 + \mathrm{MPE}/100\%} \qquad (23)$$

were computed on a daily basis from the mean ratio of GLONASS VTECs and GIM reference values for the global set of test sites. These were subsequently applied with a 1-day lag for computing corrected GLONASS model VTECs that roughly remove possible epoch-dependent scale errors. The resulting performance provides an indication of the correction quality that might be achieved, if adaptation coefficients were computed by the GLONASS control segment based on a regular TEC monitoring, rather than using only the observed flux and the geomagnetic indices. In the analysis period of the present study, c_A values ranging from roughly 0.5 to 2.0 with a mostly seasonal dependence were obtained.

Aside from the GLONASS ionosphere model, the aforementioned error metrics were likewise evaluated for the GPS (Klobuchar) and Galileo (NeQuick-G, NTCM-G) ionospheric correction models. Klobuchar model coefficients and Galileo effective ionization levels as transmitted by the respective constellations on the days of interest, were taken from the BRD400DLR combined multi-GNSS navigation data files in RINEX 4 format (Montenbruck and Steigenberger 2022) (from 2021) and its RINEX 3 predecessors (until 2020).

Table 2 VTEC error statistics of individual ionosphere models relative to IGS GIMs in 2024 based on 30 test sites (CDMA: activity data from GLONASS CDMA navigation message; SPWC: space weather center data; adj: daily adjustment of the adaptation coefficient; LNAV: GPS legacy navigation message; INAV: Galileo E1/E5b integrity navigation message)

Model	Activity Ind	ME	MAE	MPE	MAPE
GLONASS	CDMA	− 0.8	15.4	− 1.5	49.0
GLONASS	SPWI	0.0	16.0	− 0.1	50.5
GLONASS	CDMA, adj	− 0.3	13.1	0.7	42.8
GLONASS	SPWC, adj	− 0.2	13.5	0.9	44.0
Klobuchar	LNAV	− 9.0	12.3	− 16.0	39.8
NeQuick-G	INAV	− 4.2	8.0	− 10.5	26.8
NTCM-G	INAV	− 3.8	7.4	− 5.5	27.4

Results and discussion

For a first analysis, VTEC predictions from the GLONASS model are compared in Table 2 with the corresponding IGS GIM values for the year 2024, in which solar flux and geomagnetic activity parameters could be obtained from the GLONASS navigation message. Within this year of very high solar activity and overall TEC, the GLONASS model shows a small bias of less than 1 TECU, but generally larger mean absolute errors than the GPS and Galileo ionosphere models. At the given overall error level, only a marginal performance difference can be observed when feeding the model with observed space weather data rather than those transmitted in the navigation message, which is consistent with the reasonable overall agreement of both data sets as discussed above (Fig. 3).

On the other hand, a clear MAPE reduction can be observed, when adjusting the adaptation coefficient based on the ratio of modeled and observed (GIM) VTECs of the preceding day. Upon scaling the modeled values with this factor, MAPE values of about 44% are achieved, which represent an error correction performance of about 56%. This is similar to the Klobuchar model but clearly falls behind the NeQuick-G and NTCM-G models, which both enable corrections at a level of better than 70%. Also, in terms of mean absolute errors, the latter models clearly outperform the GLONASS model. At MAEs of about 13 TECU (following the c_A adjustment), the vertical delay predictions exhibit errors of about 2 m at the L1 frequency. This results in representative slant delay errors of about 4 m (for an average mapping function of 2) and positioning errors at the level of 10 m for an assumed position dilution of precision (PDOP; Langley et al. 2017) of 2.5. With MAEs of less than

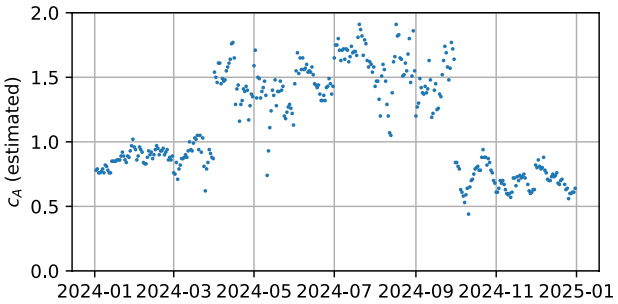

Fig. 6 Daily estimates of GLONASS adaptation coefficients based on the ratio of model predictions and GIM VTECs

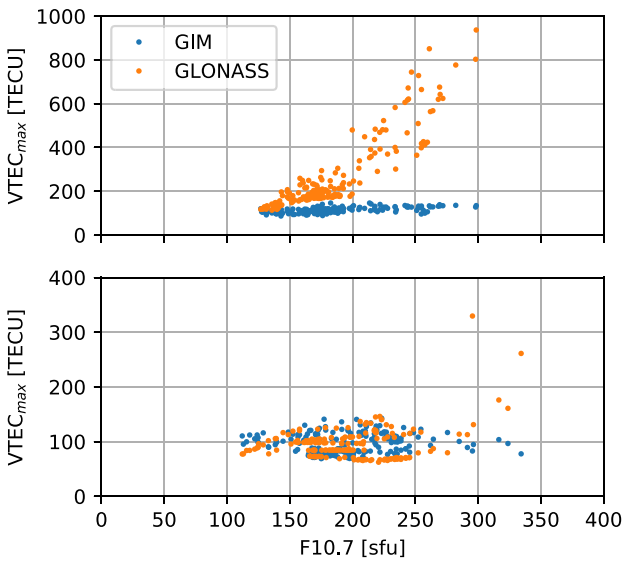

Fig. 7 Daily peak VTEC values across the 30 test sites for global ionosphere maps (GIMs) and predictions of the GLONASS model in 2024 based on space weather service center values of $F_{10.7}$ and A_p. Top: January to March and October to December 2024; bottom: April to September

8 TECU, the corresponding errors of the Galileo models are smaller by more than one third.

A time series of daily adaptation coefficients estimated from the average ratio of nominal GLONASS model predictions (using the broadcast activity parameters with $c_A = 1$) and the IGS GIM VTECs at the 30 test sites is shown in Fig. 6. The values cover a range of roughly 0.5–2.0 and exhibit a small day-to day scatter with quasi-periodic, monthly variations for most of the year. On top of these, pronounced discontinuities at the beginning of April and October may be noted with roughly two times higher c_A values in the summer months as compared to the winter season (of the northern hemisphere). The smaller, monthly variations can essentially be attributed to the specific choice of model functions (Eq. 2) for the seasonal dependence of the peak electron density, which are formulated in terms of the integer-valued calendar month and thus cause a varying model error in the course of each month.

The summer/winter disparity, on the other hand, is evidently related to the choice of different formulations of the top-layer scale height B_{top} for the October-to-March and April-to-September periods. These were originally developed for the NeQuick-1/G models, which build on monthly $f_{0,\text{F2}}$, and $M(3000)_{\text{F2}}$ tables of the International Telecommunications Union (ITU) for computing the F2-layer peak electron density $N_{\text{max,F2}}$. On the other hand, pronounced discontinuities in the modeled electron density arise at the transition between the different B_{top} formulations, when working with the analytical $N_{\text{max,F2}}$, $f_{0,\text{F2}}$, and $M(3000)_{\text{F2}}$ expressions in the GLONASS model.

Particular problems with the top layer modeling of the GLONASS model can be noted in the October-to-March time frame at high solar flux values. This is illustrated in Fig. 7, which compares the daily peak values of VTECs computed with the GLONASS model with the respective GIM values for a year of high solar activity (2024). Computations are based on solar-geomagnetic values from space weather service centers, which cover higher peak values of $F_{10.7}$ than the GLONASS broadcast ionosphere parameters.

While a fair match is found in the summer season, excessively large and highly unrealistic peak VTECs for selected sites and local times are predicted in the winter months by the GLONASS model for solar flux values beyond 200 sfu. These suggest that the empirical relations for the geographical variation of the maximum F2 layer density in the GLONASS model (see Eq. (2)) have been derived over a smaller range of solar flux values and exhibit notable deficiencies at extreme solar activity.

A long-term comparison of the GLONASS model with GPS and Galileo ionospheric correction models over the duration of one solar cycle is shown in Fig. 8. It starts and ends near solar maxima (2014, 2024) with representative $F_{10.7}$ values of 150–250 sfu, while the central years around 2019 represent solar minimum conditions with flux values at the level of 70 sfu. Compared to IGS GIMs, the GLONASS model exhibits small VTEC biases within ±2 TECU at all phases of the solar cycle. Mean absolute VTEC errors are comparable to those of the Klobuchar model and range from about 5 TECU in quiet years to roughly 16 TECU at high solar activity, but the annual mean relative errors do not grow excessively in quiet years and are confined to mostly less than 21%. The corresponding MAPE values range from roughly 47% (high activity) to 63% (low activity).

As discussed above, only minor performance differences were observed when comparing GLONASS model predictions based on broadcast values of solar flux and geomagnetic activity with those based on observed activity values from space weather centers (Table 2). However, a

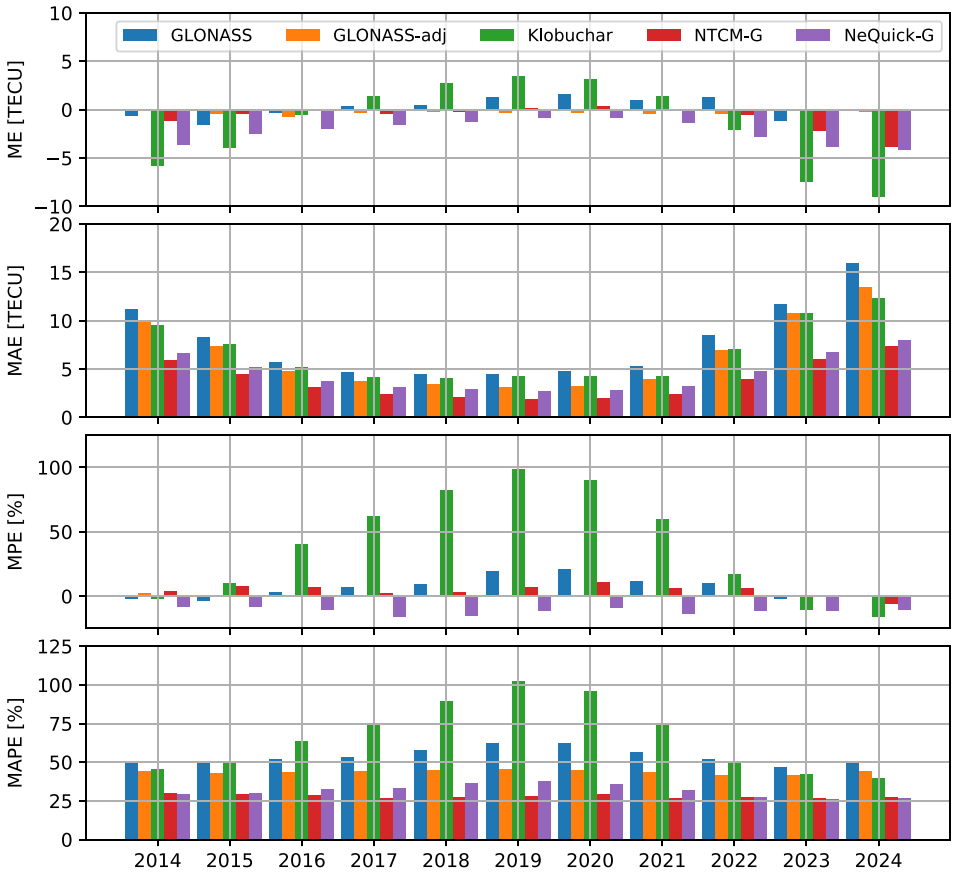

Fig. 8 VTEC errors of individual ionosphere models relative to IGS GIMs for the years 2014 to 2024

clear reduction of both the mean absolute (3–13 TECU) and mean absolute percentage errors (41–45%) is achieved when adjusting the adaptation coefficient of the GLONASS model based on the daily mean ratio of predicted and observed VTEC values. However, even with data ingestion, the GLONASS model does not reach the prediction performance of the Galileo NeQuick-G and NTCM-G models. Making use of the effective ionization level determined by the Galileo control segment and transmitted in the navigation message, both of these models provide TEC predictions closely aligned to actual slant TEC measurements at the Galileo sensor stations. The resulting VTEC errors are similar for both models and range from 2 to 8 TECU (MAE) and 26–37% (MAPE) throughout the solar cycle.

The results presented here are in good qualitative agreement with earlier analyses of the GLONASS, Klobuchar and NeQuick-G models reported in Yasyukevich et al. (2023), but show some differences (of up to about 5% in MAPE) in the quantitative performance metrics for the overlapping analysis period (2014–2020). As a general trend, slightly better performance metrics are obtained for the GLONASS model in that work, while NeQuick-G shows a somewhat lower performance than given in Fig. 8. Part of these differences can be attributed to a smaller set of test sites in Yasyukevich et al. (2023), but it remains unclear, whether or to what extent different sets of model input parameters or implementation aspects of the various models contribute to the observed inconsistencies. In any case, these uncertainties do not affect the overall ranking of the three models, with Galileo consistently outperforming both GLONASS and GPS in terms of VTEC correction capability in both studies.

Summary and conclusions

Along with the continued space segment modernization and the introduction of new CDMA signals, the Russian GLONASS has introduced a global electron density model for ionospheric correction in single-frequency positioning. The model inherits various elements of the NeQuick model family, but uses purely analytical formulations without tabular data for describing the geographical and temporal variation of the F2 peak electron density, as well as a pair of semi-Epstein layers for describing the vertical density profile. By limiting itself to the F2 layer contribution, the model is generally more simple than NeQuick but allows for a semi-analytical integration of the vertical TEC. As such, it can both be used as a full 3D electron density model for slant TEC modeling by numerical integration and as a computationally efficient 2D single-layer model for terrestrial and

aeronautical applications. Solar flux values and geomagnetic activity values for the GLONASS ionosphere model are presently transmitted by a subset of the active GLONASS-M+, -K1, and -K2 satellites as part of the L3OC and L1OC navigation messages.

A comprehensive comparison of predicted VTEC values with global ionosphere maps over the duration of a full solar cycle demonstrates that the GLONASS model is largely free of TEC biases and does not exhibit pronounced relative errors in quiet periods that are characteristic for the GPS Klobuchar model. In terms of mean absolute percentage errors or, equivalently, correction performance, the GLONASS model offers advantages during periods of low solar activity and a similar performance at high activity. While not currently exploited by the GLONASS control segment, an obvious performance benefit evidenced by a 5–10% MAPE reduction can be achieved when using adjusted values of the "adaptation" coefficient. It acts as a global scaling factor for the TEC predicted by the model with the actual solar flux and geomagnetic activity parameters and can be used to better align the modeled values with the observed ionospheric activity. Among others, systematic errors introduced by different expressions for the top layer scale height in the winter and summer seasons can be alleviated in this manner. However, unreasonably large VTEC may still be predicted during the winter period (October to March) at high solar flux values due to improperly matched models for the $F_{10.7}$ dependence of the F2-layer maximum electron density and the top layer scale height in these months.

While the GLONASS model appears attractive in view of its flexible use as a 2D or 3D model, it is not, however, competitive with the ionospheric correction models and broadcast activity parameters of the Galileo system. These offer a representative VTEC correction capability of 70% in both the 3D version (NeQuick-G) and the 2D version (NTCM-G), which clearly outperforms the accuracy of the GLONASS model. Even though the 3D GLONASS model formulation offers a roughly four-times lower computational effort than NeQuick-G, it is hardly a viable alternative for those users requiring a fully 3-dimensional description of the electron density (e.g., for STEC computation on orbiting vehicles). The much leaner 2D formulation, in contrast, shows a similar computational burden as NTCM-G, but a roughly 1.5-times lower correction capability.

Acknowledgements The authors are grateful to Peter Mumford, Craig Roberts, and Russell Commins for their continued effort in operating the UNSW GNSS monitoring station. JAVAD GNSS Europe is acknowledged for the provision of a prototype firmware supporting L1OC, L2OC, and L3OC tracking as well as recording of raw navigation data frames. GNSS navigation messages and global ionosphere maps used in the present study have been prepared by the International GNSS Service (IGS), while space weather data were collected, prepared, and publicly released by the Helmholtz Centre for Geosciences (GFZ) in cooperation with the Dominion Radio Astrophysical Observatory and Natural Resources Canada. The support of all institutions is gratefully acknowledged.

Author's contributions OM proposed the study concept, prepared the draft manuscript, and conducted selected analyses. CPG provided the prototype s/w implementation of the GLONASS ionosphere model and contributed to the performance analyses and model comparisons, as well as the art work. PS built up the monitoring stations for the GLONASS CDMA signal reception, developed the decoders for CDMA message decoding, and maintained the GLONASS navigation data archive used for this study. All authors critically reviewed the final manuscript.

Funding Open Access funding enabled and organized by Projekt DEAL. Open Access funding enabled and organized by Projekt DEAL, an initiative of the Alliance of Science Organisations in Germany.

Availability of data and material IGS global ionosphere maps and GNSS navigation data as used in this study are publicly available from the global IGS data centers, such as CDDIS (https://cddis.nasa.gov/archive/gnss/data/). Space weather data are shared by GFZ at https://kp.gfz.de/en

Declarations

Conflict of interest The authors have no Conflict of interest that are relevant to the content of this article.

References

Bidaine B, Warnant R (2010) Assessment of the NeQuick model at mid-latitudes using GNSS TEC and ionosonde data. Adv Space Res 45(9):1122–1128. https://doi.org/10.1016/j.asr.2009.10.010

Bilitza D, Pezzopane M, Truhlik V, Altadill D, Reinisch BW, Pignalberi A (2022) The International Reference Ionosphere model: a review and description of an ionospheric benchmark. Rev Geophys 60(4):e2022RG000792. https://doi.org/10.1029/2022RG000792

CSNO (2017) BeiDou navigation satellite system signal in space interface control document: Open service signal B1C, issue 1.0, Dec. 2017, China Satellite Navigation Office. http://en.beidou.gov.cn/SYSTEMS/ICD/201806/P020180608519640359959.pdf

EU (2016) European GNSS (Galileo) Open Service, ionospheric correction algorithm for Galileo single frequency users, issue 1.2, European GNSS Service Centre (GSC). https://www.gsc-europa.eu/sites/default/files/sites/all/files/Galileo_Ionospheric_Model.pdf

EU (2022) European GNSS (Galileo) Open Service, NTCM-G ionospheric model description, issue 1.0, May 2022, European GNSS Service Centre (GSC). https://www.gsc-europa.eu/sites/default/files/NTCM-G_Ionospheric_Model_Description_-_v1.0.pdf

GFZ (2025) Geomagnetic planetary three-hour index Kp and associated geomagnetic indices as well as relevant solar indices. https://kp.gfz.de/app/files/Kp_ap_Ap_SN_F107_since_1932.txt

Gini F (2024) RINEX, The Receiver Independent Exchange Format, Version 4.02. https://files.igs.org/pub/data/format/rinex_4.02.pdf

Hernández-Pajares M, Juan JM, Sanz J, Orus R, Aragón-Àngel A, Garcia-Rigo A, Feltens J, Komjathy A, Schaer SC, Krankowski A (2009) The IGS VTEC maps: a reliable source of ionospheric information since 1998. J Geod 83(3–4):263–275. https://doi.org/10.1007/s00190-008-0266-1

Hoque MM, Jakowski N, Orús-Pérez R (2019) Fast ionospheric correction using Galileo Az coefficients and the NTCM model. GPS Solut 23(2):41. https://doi.org/10.1007/s10291-019-0833-3

Ivanov V, Zatolokin D, Gorbachev O (2017) Comparing models of total electron content in the ionosphere for GLONASS. Gyroscopy Navigat 8:295–299. https://doi.org/10.1134/S2075108717040071

Johnston G, Riddell A, Hausler G (2017) The International GNSS Service. In: Teunissen PG, Montenbruck O (eds) Springer Handbook of Global Navigation Satellite Systems. pp 967–982. Springer, Cham. https://doi.org/10.1007/978-3-319-42928-1_33

Klobuchar JA (1987) Ionospheric time-delay algorithm for single-frequency GPS users. IEEE Trans Aerospace Elec Syst AES 23(3):325–331. https://doi.org/10.1109/TAES.1987.310829

Klobuchar JA, Kunches JM (2003) Comparative range delay and variability of the earth's troposphere and the ionosphere. GPS Solut 7(1):55–58. https://doi.org/10.1007/s10291-003-0047-5

Langley R, Teunissen P, Montenbruck O (2017) Introduction to GNSS. In: Teunissen P, Montenbruck O (eds) Springer Handbook of Global Navigation Satellite Systems. pp 3–23. Springer, Cham. https://doi.org/10.1007/978-3-319-42928-1_1

Laundal KM, Richmond AD (2017) Magnetic coordinate systems. Space Sci Rev 206(1):27–59. https://doi.org/10.1007/s11214-016-0275-y

Leitinger R, Zhang ML, Radicella SM (2005) An improved bottomside for the ionospheric electron density model NeQuick. Ann Geophys 48(3):525–534. https://doi.org/10.4401/ag-3217

Li W, Wang K, Yuan K (2023) Performance and consistency of final global ionospheric maps from different IGS analysis centers. Remote Sens 15(4):1010. https://doi.org/10.3390/rs15041010

Matzka J, Stolle C, Yamazaki Y, Bronkalla O, Morschhauser A (2021b) The geomagnetic Kp index and derived indices of geomagnetic activity. Space Weather 19(5):e2020SW002641. https://doi.org/10.1029/2020sw002641

Matzka J, Bronkalla O, Tornow K, Elger K, Stolle C (2021a) Geomagnetic Kp index, version 1.0. GFZ Data Service. https://doi.org/10.5880/Kp.0001

Milanowska B, Wielgosz P, Wang N, Hoque MM, Tomaszewski D, Jarmołowski W, Krypiak-Gregorczyk A, Krzykowska-Piotrowska K, Rapiński J (2025) Evaluation of ionospheric correction models in multi-GNSS single-frequency SPP. Adv Space Res 76(2):914–925. https://doi.org/10.1016/j.asr.2025.04.050

Montenbruck O, González Rodríguez B (2020) NeQuick-G performance assessment for space applications. GPS Solut 24(1):13. https://doi.org/10.1007/s10291-019-0931-2

Montenbruck O, Steigenberger P (2022) BRD400DLR: DLR's merged multi-GNSS broadcast ephemeris product in RINEX 4.00 format; DLR/GSOC. https://doi.org/10.57677/BRD400DLR

Nava B, Coisson P, Radicella S (2008) A new version of the NeQuick ionosphere electron density model. J Atmos Solar-Terr Phys 70(15):1856–1862. https://doi.org/10.1016/j.jastp.2008.01.015

Orús R, Hernández-Pajares M, Juan J, Sanz J, Garcıa-Fernández M (2002) Performance of different TEC models to provide GPS ionospheric corrections. J Atmos Solar-Terr Phys 64(18):2055–2062. https://doi.org/10.1016/S1364-6826(02)00224-9

Roma-Dollase D, Hernández-Pajares M, Krankowski A, Kotulak K, Ghoddousi-Fard R, Yuan Y, Li Z, Zhang H, Shi C, Wang C et al (2018) Consistency of seven different GNSS global ionospheric mapping techniques during one solar cycle. J Geod 92:691–706. https://doi.org/10.1007/s00190-017-1088-9

Russian Space Systems (2016a) GLONASS Interface Control Document: Code division multiple access open service navigation signal in L1 frequency band, edition 1.0. https://web.archive.org/web/20220121130245/https://russianspacesystems.ru/wp-content/uploads/2016/08/ICD-GLONASS-CDMA-L1.-Edition-1.0-2016.pdf

Russian Space Systems (2016b) GLONASS Interface Control Document: Code division multiple access open service navigation signal in L3 frequency band, edition 1.0. https://web.archive.org/web/20220121130303/https://russianspacesystems.ru/wp-content/uploads/2016/08/ICD-GLONASS-CDMA-L3.-Edition-1.0-2016.pdf

Russian Space Systems (2016c) GLONASS Interface Control Document: General description of code division multiple access signal system, edition 1.0. https://web.archive.org/web/20220121130328/https://russianspacesystems.ru/wp-content/uploads/2016/08/ICD-GLONASS-CDMA-General.-Edition-1.0-2016.pdf

SSC (2022) Navstar GPS Space Segment/Navigation User Segment Interfaces, IS-GPS-200N, Space Systems Command. http://www.gps.gov/technical/icwg/IS-GPS-200N.pdf

Steigenberger P, Montenbruck O, Hauschild A (2024) Antenna and attitude modeling of modernized GLONASS satellites. Adv Space Res 74(7):3045–3059. https://doi.org/10.1016/j.asr.2024.07.001

Tapping KF (2013) The 10.7 cm solar radio flux (F10.7). Space Weather 11(7):394–406. https://doi.org/10.1002/swe.20064

Wang N, Li Z, Yuan Y, Huo X (2021) BeiDou global ionospheric delay correction model (BDGIM): performance analysis during different levels of solar conditions. GPS Solut 25(3):97. https://doi.org/10.1007/s10291-021-01125-y

Wielgosz P, Milanowska B, Krypiak-Gregorczyk A, Jarmołowski W (2021) Validation of GNSS-derived global ionosphere maps for different solar activity levels: case studies for years 2014 and 2018. GPS Solut 25(3):103. https://doi.org/10.1007/s10291-021-01142-x

Xu H, Li M, Yuan Y, Zhang T, Zhang W (2025) Performance of BDGIM, Klobuchar, NTCM-G and NeQuick-G models during 25th solar cycle. Adv Space Res 75(10):7654–7667. https://doi.org/10.1016/j.asr.2025.02.053

Yasyukevich Y, Zatolokin D, Padokhin A, Wang N, Nava B, Li Z, Yuan Y, Yasyukevich A, Chen C, Vesnin A (2023) Klobuchar, NeQuickG, BDGIM, GLONASS, IRI-2016, IRI-2012, IRI-Plas, NeQuick2, and GEMTEC ionospheric models: a comparison in total electron content and positioning domains. Sensors, 23. https://doi.org/10.3390/s23104773

Oliver Montenbruck is an honorary professor at Technische Universität München (TUM) and former head of the GNSS Technology and Navigation Group at DLR's German Space Operations Center. His research interests comprise space-borne GNSS receiver technology, GNSS-based autonomous navigation systems, precise orbit determination, multi-constellation GNSS, and LEO PNT systems.

Claudio Price Gonzalez received his master in Earth Oriented Space Science and Technology from Technische Universität München (TUM) in 2025. As part of his MSc thesis, he studied the GLONASS ionosphere model and conducted a comprehensive performance analysis.

Peter Steigenberger received his master and PhD degrees in Geodesy from Technische Universität München (TUM) in 2002 and 2009, respectively. Currently, he is a senior researcher at DLR's German Space Operations Center (GSOC) and chairs the IGS Multi-GNSS Pilot Project. His research interests focus on GNSS data analysis, in particular precise orbit and clock determination of GNSS satellites and the evolving navigation systems Galileo, BeiDou, and QZSS.